PERGAMON

Vision Research 39 (1999) 2987–2998

Vision Research

www.elsevier.com/locate/visres

Quantitative estimations of foveal and extra-foveal retinal circuitry in humans

Johan Sjöstrand [a,*], Viktoria Olsson [a], Zoran Popovic [a], Nils Conradi [b]

[a] *Department of Ophthalmology, Göteborg University, Sahlgrenska University Hospital, S-413 45 Göteborg, Sweden*
[b] *Department of Pathology, Göteborg University, Sahlgrenska University Hospital, S-413 45 Göteborg, Sweden*

Received 29 December 1997; received in revised form 30 December 1998

Abstract

For an understanding of the basis for psychophysical measurement of visual resolution, quantitative morphological studies of retinal neuronal architecture are needed. Here we report on cell densities and retinal ganglion cell:cone ratio (RGC:C) from the foveal border to the peripheral retina (34° eccentricity). Quantitative estimates of RGC and C densities were made using a modified disector method in three vertically sectioned human retinae and were adjusted for RGC displacement. In agreement with our previous data on humans, we found an RGC:C ratio close to 3 at 2–3° eccentricity. Outside the foveal border, the ratio declined to 1.0 at 7.5° eccentricity and to 0.5 at eccentricities larger than 19°. Center-to-center separation of C and RGC in addition to center-to-center separation of estimated 'receptive fields' was calculated at corresponding locations along the superior and inferior hemimeridians. The center-to-center separation of estimated 'receptive fields' was found to be more closely related to resolution thresholds from the fovea to 19° eccentricity than was the separation of RGC and C. On the basis of these quantitative estimates, models for neural circuitry involved in central and peripheral spatial vision can be discussed.

Keywords: Ganglion cell topography; Displaced amacrine cells; Cell separation; Resolution; Retinal circuitry; Cones; Retinal cells

1. Introduction

Studies on experimental animals have increased our knowledge about the physiology and morphology of the retina (cf. Rodieck, 1998). However, important aspects of vision in humans, such as spatial resolution can only be analyzed by psychophysical measurements. For an understanding of the relations between spatial resolution and the different populations of photoreceptors and retinal ganglion cells (RGC), quantitative morphological studies of the human retina are essential. The sampled retinal image is processed by different populations of ganglion cells, each of which has a physiologically defined receptive field. A major goal is to provide numerical densities of these receptive fields. This requires knowledge of the cone photoreceptor and ganglion cell densities and of their topography and convergence. Three features of the human retina complicate the evaluation of retinal circuity: (1) lateral displacement of central RGC; (2) existence of different RGC types (Rodieck, Binmoeller & Dineen, 1985; Kolb & Dekorver, 1991; Kolb, Linberg & Fisher, 1992; Dacey & Petersen, 1992; Grünert, Greferath, Boycott & Wässle, 1993); and (3) the existence of displaced amacrine cells in the RGC layer. Lateral displacement of RGC means that cones at a given eccentricity make contact with RGC at greater eccentricities via fibers of Henle and bipolar cells (see below). The consequence is that a group of RGC connected to centrally located cones are distributed over a larger area than the corresponding cones (Schein, 1988 e.g. see Fig. 3b). Within the fovea information from one foveal cone is thought to be transmitted to two midget RGC, one ON-center and one OFF-center type of cell. Under such conditions this system should show a retinal ganglion cell:cone ratio (RGC:C) of 2. However, it is difficult to separately estimate the densities of ON-center and OFF-center midget RGC since other types of RGC, such as parasol cells, are not easily excluded from the estimates. Displaced amacrine cells are cells with the characteris-

* Corresponding author. Fax: +46-31-412904.

0042-6989/99/$ - see front matter
PII: S0042-6989(99)00030-9

tics of amacrine cells that lie within the RGC layer. These cells should be excluded, since they are not directly involved in the cellular chain from receptors to target cells in relay stations and the visual cortex. Most displaced amacrine cells are GABA-ergic (about 90% in the monkey) (Wässle, Grünert, Röhrenbeck & Boycott, 1990; Koontz, Hendrickson, Brace & Hendrickson, 1993) and therefore possible to stain by immunohistochemistry.

Detailed analyses of sampling densities of RGC have been carried out in the non-human primate fovea (Schein, 1988; Wässle et al., 1990; Martin & Grünert, 1992) and neuroanatomical circuitries of the primate retina have been presented (Wässle et al., 1990; Martin & Grünert, 1992; Wässle, Grünert, Martin & Boycott, 1994). Recent primate morphometric data indicate that three to four ganglion cells are present for every foveal cone (Wässle et al., 1990).

Estimates of cell densities in human whole mount retinas have been made by Curcio and coworkers (Curcio, Sloan, Kalina & Hendrickson, 1990; Curcio & Allen, 1990; Dacey, 1993). In addition, RGC and C density data of one human fovea sectioned along the vertical meridian has been reported (Sjöstrand, Conradi & Klarén, 1994). Previous estimates of RGC:C ratio in humans have been based on assumptions since detailed data on displacement of RGC subserving foveal cones are lacking. Curcio and Allen (1990) interpreted their data on C and RGC densities as compatible with a ratio of 2:1 over a wider retinal area or 3:1 if confined to the foveal center. Sjöstrand et al. (1994), using size-adjusted displacement data of macaques (Schein, 1988) and cell densities of one human retina, calculated an RGC:C ratio of approx. 3 at the foveal border. A ratio larger than 2 is a prerequisite for each foveal cone to have separate connections to one ON-center and one OFF-center midget RGC in addition to connections to other RGC types.

In the present study our aim was to extend the analysis of RGC:C ratio and of changes in cell separation from the fovea to peripheral retina. We wanted to test the hypothesis that there are sufficient numbers of RGC to supply cones with ON and OFF types of RGC. By assuming that the decrease in RGC:C ratio outside the fovea only depends on increasing cone convergence we could define the cone area from which one RGC receives information as the estimated 'receptive field'. We evaluated whether the estimated center-to-center separation of 'receptive fields' shows a closer correspondence to measured spatial resolution than separation of RGC and C. The RGC displacement was taken into account in order to compensate RGC densities for the differences in area occupied by RGC versus corresponding C ('effective' RGC density). Concerning the existence of different populations of RGC, we based our modeling of RGC separation versus resolution thresholds on the assumption that a majority of RGC in the human retina are concerned with the geniculostriate pathway as in macaque monkeys (Perry & Cowey, 1984). We have used the disector method to separately count displaced amacrine cells stained by GABA-immunohistochemistry and eliminated them from the total number of RGC.

2. Methods

2.1. Case descriptions

Three eyes were examined. The specimens were obtained after surgery for maxillary carcinoma and were fixed within a few minutes after enucleation. The patients were 39 (Case 1), 73 (Case 2) and 49 (Case 3) years of age at the time of surgery. The carcinoma did not affect the eye or the optic nerve and visual acuity preoperatively was 1.0 or better in all cases. No history of eye disease was present in any of the cases.

Case 1 was included in our previous reports on densities of retinal ganglion cells (Conradi & Sjöstrand, 1993; Sjöstrand et al., 1994). This eye was fixed in 3% glutaraldehyde and 3% formaldehyde. Retinal strips taken along both sides of the vertical hemimeridian were embedded in epoxy or acrylic resin. Cell counts from 0.8 to 9.0 mm eccentricity were made above and below the foveal center.

The eyes of Cases 2 and 3 (49 and 72 years of age respectively) were fixed in 2% formaldehyde and 0.5% glutaraldehyde. The retinal strips were embedded in acrylic resin. Cell counts were made along the superior and inferior hemimeridians from 0.6 to 9.0 mm eccentricity.

2.2. Histochemistry and immunocytochemistry

In Case 1, RGC and C were counted using sections stained with methylene blue/toluidine blue. Immunocytochemistry for the identification of displaced amacrine cells was unsuccessful due to the fixation and/or embedding procedure. On the other hand, separation of cone and rod nuclei on the basis of localization and nuclear chromatin was relatively easy (Fig. 1).

In Cases 2 and 3, GABA-ergic amacrine cells were stained (Fig. 2a) using an anti-GABA rabbit antibody (diluted 1:1000, Sigma Immunochemicals). All sections were blocked for endogenous peroxidase. All stains were performed on an automatic immunostainer (Dako Techmate 1000) using a biotinylated secondary goat-anti-rabbit antibody, peroxidase-conjugated streptavidin (Dako Chemmate) and DAB as chromogen, all supplied as standard solutions (Dako Chemmate). Amacrine cells and fibers of the inner plexiform layer served as positive internal controls for GABA immuno-

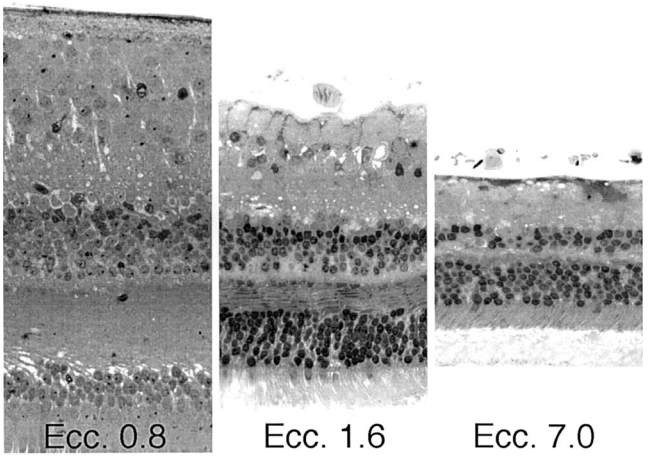

Fig. 1. Digital micrographs illustrating the morphology of the retina at 0.8 (epoxy resin, Case 1), 1.6 and 7.0 (acrylic resin, Case 2 and 3) mm eccentricity, respectively. Note distinct nuclear morphology of cones in Case 1 as compared to Case 2 and 3 (see Fig. 2).

histochemistry of displaced amacrines. The mean percentage of displaced amacrines of the total cell count in the retinal ganglion cell layer at various eccentricities in these two cases was used in order to calculate RGC from total nerve cell counts within the ganglion cell layer in Case 1.

For the purpose of counting cone nuclei in specimens embedded in acrylic resin separate sets of sections were stained at 60°C with a modified hexamine-silver technique (Fig. 2b) using a stock solution containing 5 ml of 5% aqueous silver nitrate and 100 ml of 3% aqueous hexamine. The working solution was made by mixing 2 ml of 5% aqueous sodium borate solution with 25 ml distilled water and 25 ml of the stock hexamine-silver solution. Toning in aqueous yellow gold chloride was omitted—for full description see Bancroft and Cook (1994).

2.3. Counting technique

Continuous retinal strips were taken along the superior and/or inferior vertical hemimeridians; the vertical meridian refers to the line that passes through the foveal center perpendicular to a line through the fovea and optic disc. The strips were measured before and after embedding. Blocks were cut from the strips to allow measurement from 0.6 to 9.0 mm eccentricity. Serial sections, 1 μm thick, were taken from each block. The section thickness was controlled by the small-fold-technique. In order to obtain sufficient numbers of cells in the periphery, counting frames were added symmetrically on each side of the first. In general, between 16 and 64 disectors were used.

Estimated length shrinkage during dehydration and embedding, made by comparing blocks and tissue sections, was less than 5%. Changes in tissue volume during the whole fixation to embedding process could not be determined. In studies on brain tissue where this has been carefully measured, the whole process resulted in zero volume change (Eins & Wilhelms, 1976). Hence, no compensation was made for the shrinkage caused by dehydration/embedding only.

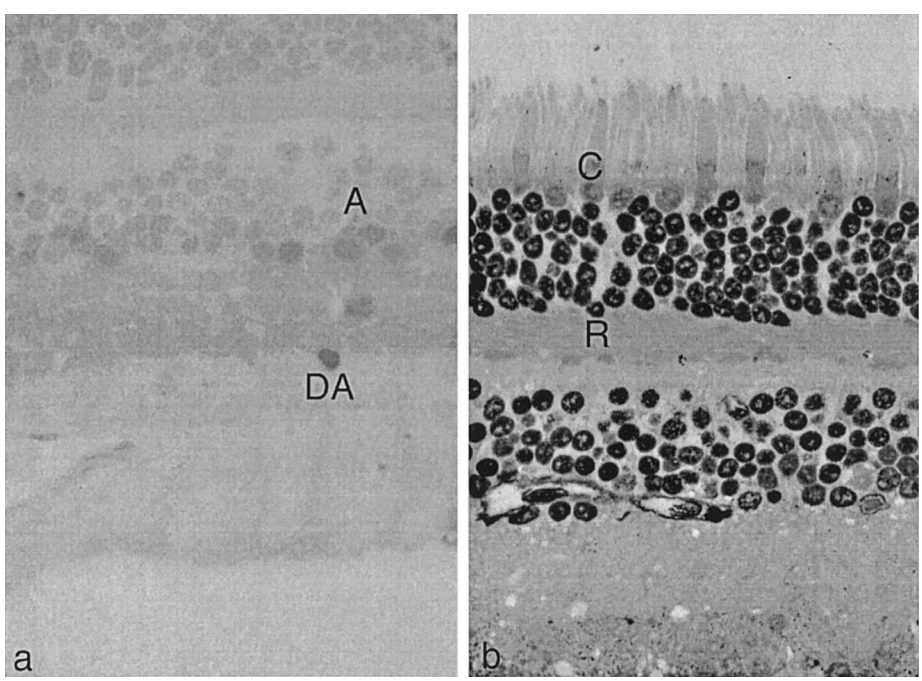

Fig. 2. Micrographs illustrating (a) staining of displaced amacrine (DA) and amacrine (A) cells by GABA-immunohistochemistry and (b) difference in nuclear characteristics between cones (C) and rods (R) using the Ag-methenamine stain on acrylic resin sections.

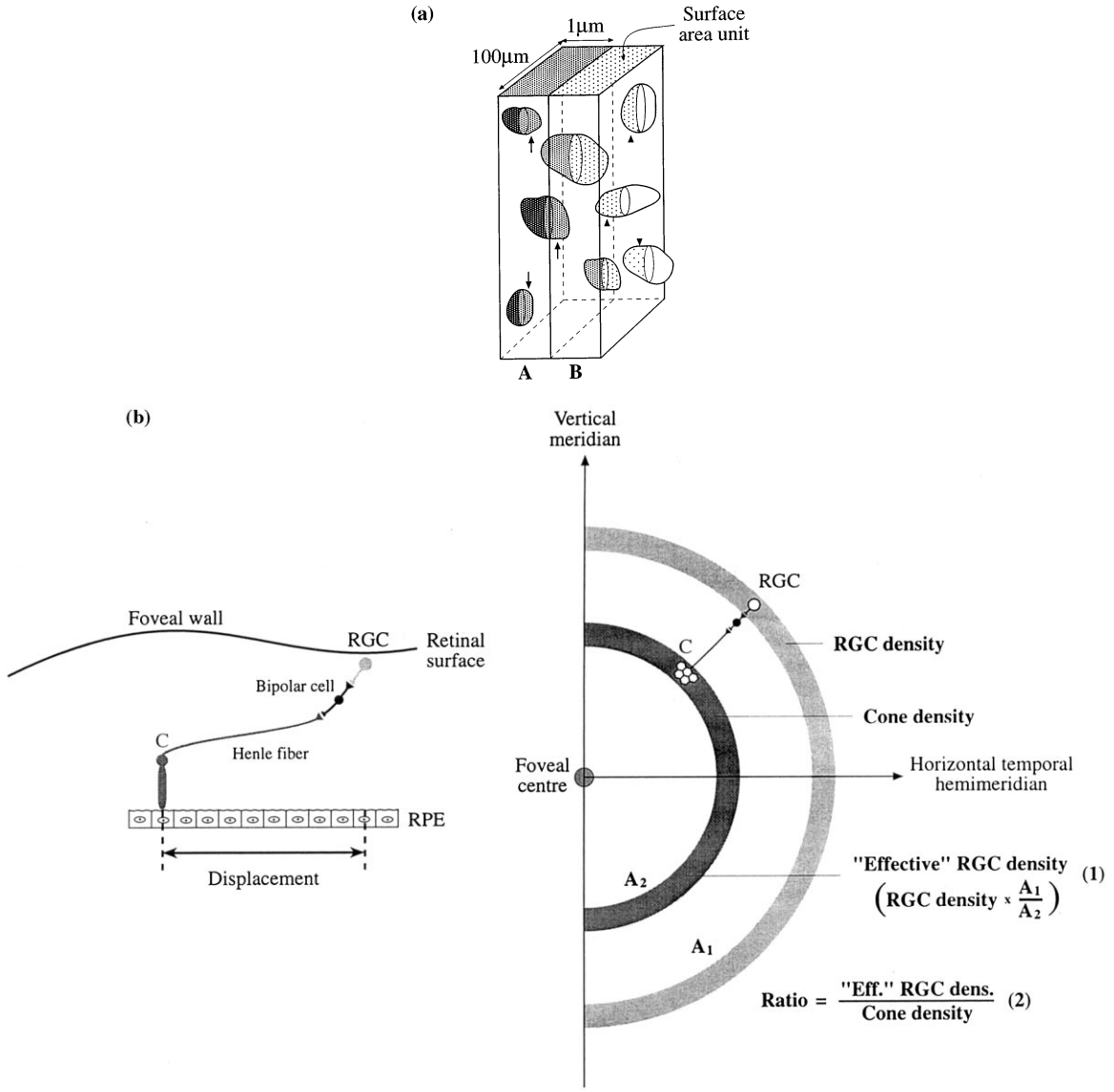

Fig. 3. Drawings of (a) the modified disector used for cell counting within a surface area unit of 100 μm^2 and (b) the calculation of 'effective' RGC density (1) and RGC:C ratio (2) (cf. Section 2). In (a), counting of cell nuclei per surface area unit will result in three nuclei (arrows) with A as reference and B as look-up section, and three nuclei (arrowheads) using B as reference and A as look-up section. In (b), the foveal retina as seen in a vertical section is schematically illustrated to the left. As can be seen, the extension of the Henle fiber results in lateral displacement of the connected RGC. To the right, the effect of lateral displacement on the retinal surface area occupied by C and connected RGC is shown. The transformations used to compensate for lateral displacement of RGC and resulting differences in the actual area (A_1), occupied by RGC, and the effective area (A_2), defined by corresponding C, are illustrated. The RGC:C ratio was calculated by dividing 'effective' RGC density by cone density.

Cells were counted using a modified disector method, Fig. 3a (Sterio, 1984). The counting was made on digital images acquired at an objective magnification of $\times 100$ (oil immersion lens) and presented in pairs on a TV monitor. Nuclei were counted only if they were seen in one (reference) but not in the next (look-up) section (Fig. 3a). The counting frame was 100 μm wide and the section thickness was 1.0 μm. Thus the area of retinal surface included in each disector was 100 (counting frame width) $\times$ 1 mm^2 (section thickness), (or 10^{-4} mm^2). By using this modified disector the number of cells per retinal surface area (N/mm^2) could be estimated (Fig. 3a). Means of cell densities and standard errors of the mean (S.E.M.) for each eccentricity are shown in Table 1.

RGC displacement was estimated in the following way. The axial offset due to the extension of the fiber of Henle from the cone cell body to the pedicles was measured by light microscopy in stained 1 μm sections cut along the vertical meridian through the center of the fovea in Case 1 and 2. Displacement due to bipolar cells was estimated by measuring the obliquely running

Table 1
Cell densities versus eccentricity[a]

Eccentricity		Density (cells/mm^2)					
mm	Degree	Cones			RGC		
		Case 1	Case 2	Case 3	Case 1[b]	Case 2	Case 3
0.6	2.2	19300[c]	16786 (1510)	24167 (4167)[d]	50600[c]	45000 (3340)	35400 (2999)[d]
0.8	3.0	12619 (1323)	14677 (1520)	16500 (1661)	38566 (3190)	39688 (3661)	34219 (2699)
1.6	6.0	11500 (1462)	10625 (1371)	11129 (1303)	19800 (2012)	20455 (2415)	19063 (1819)
2.4	9.0	7813 (1167)	8182 (1271)	8409 (1377)	9213 (1268)	6563 (897)	9531 (1208)
3.0	11.2	6786 (1143)	7667 (962)	8393 (1243)	5481 (1206)	6406 (1144)	10469 (1550)
5.0	18.7	6250 (1037)	5625 (1088)	6111 (1338)	2963 (714)	3718 (685)	3043 (926)
7.0	26.2	5769 (1144)	5000 (803)	5536 (1048)	3863 (925)	2683 (989)	3906 (691)
9.0	33.7	4839 (852)	4375 (767)	5781 (913)	2209 (678)	2222 (627)	2813 (685)

[a] Mean values and (S.E.M.) data averaged from the superior and inferior vertical hemimeridian.
[b] RGC values obtained by subtracting percentage of displaced amacrines (mean, Case 2 and Case 3) from total RGC counts.
[c] From Sjostrand et al., 1994 (interpolated value).
[d] Based only on data from inferior hemimeridian due to imperfect superior specimen.

fiber bundles within the inner nuclear layer. The magnitude of total displacement (y) of ganglion cells (offsets due to cone fibers and bipolar cells added together) in the direction away from the fovea is approximated by the equation $y = -0.24x + 0.56$ ($r = 0.99$), where x is the cone eccentricity along the vertical meridian from an eccentricity of 0.6 mm. For eccentricities of 2.4 mm or more the lateral displacement was of a low degree and was therefore not included in the calculation. The displacement data are described in detail in a parallel study (Sjöstrand et al., in preparation).

2.4. Calculations

Due to lateral displacement of RGC in the fovea, the area occupied by cones is much smaller than the area occupied by the corresponding (connected) RGC (Fig. 3b). Therefore, foveal and parafoveal RGC densities had to be compensated for differences in retinal area containing connected C and RGC in order to make them comparable to those of C (Fig. 3b, cf. Schein (1988)). The transformed RGC density or 'effective' RGC density is consequently the density RGC would have if they had been located just above the cones as if no radial offset of RGC relative to cone inner segments was present (see Fig. 3b for explanation).

The ratio of RGC to C was obtained by dividing 'effective' RGC density with cone density at corresponding locations.

A hexagonal array (Snyder & Miller, 1977) was assumed in the calculation of average center-to-center separation (S) of RGC, C (Table 2) and estimated 'receptive fields'. To calculate separation, density has to be transformed to a linear parameter, inverted and compensated for hexagonal packing; thus $S = (\sqrt{3}/2d)^{1/2}$, where d is the cone (Table 1), 'effective' RGC or estimated 'receptive field' density (see Section 3 for definition). Densities were compensated for the non-linear projection of the retinal image according to Drasdo and Fowler (1974).

2.5. Resolution thresholds

Minimal angles of resolution (MAR) were measured along the vertical visual field meridian using high-pass resolution perimetry (Frisén, 1992). Single ring-shaped high-pass spatial frequency filtered targets were presented at a contrast of 0.5 and 0.25 and 50% thresholds were obtained by probit analysis and expressed in min of arc (for details see Frisén, 1992, 1995). MAR at locations corresponding to our separation data were interpolated from the measured threshold values. Resolution thresholds at each 10° off axis on the upper and lower vertical meridians out to 50° for two observers were obtained from Frisén (1992). In addition, resolution thresholds of the same observers were measured for the present study along the upper and lower vertical hemimeridians at eccentricities 0, 2.5, 6 and 10°.

3. Results

3.1. Cell densities

The measured cell densities of C and RGC expressed as mean values for eccentricities of 0.6–9.0 mm along the superior and inferior hemimeridian are presented in Table 1. At the foveal border (0.6 mm or 2.2° eccentricity) the C density varies from 17 000 to 24 000 cells/mm^2 and the RGC density varies from 35 000 to 51 000 cells/mm^2. Corresponding densities for displaced amacrine cells (Cases 2 and 3) are shown in Fig. 4. The

mean percentage of amacrines was 6% between 0.6 and 0.8 mm (2.2–3.0°), 14% between 1.6 and 2.4 mm (6.0–9.0°), 20% between 3.0 and 5.0 mm (11.2–18.7°), and 10% between 7.0 and 9.0 mm (26.2–33.7°).

3.2. 'Effective' RGC density and RGC:C ratio

The calculation of 'effective' RGC density (Table 2) was based on estimated density values adjusted for RGC displacement and areal change (cf. methods and Fig. 3b). The ratio between 'effective' RGC and C was 2.93 ± 0.57 (Fig. 5) at and near the foveal border (0.6–0.8 mm or 2.2–3.0° eccentricity). At an eccentricity of 2.4–3.0 mm (9.0–11.2°) the RGC:C ratio was approx. 1. From an eccentricity of 5.0 mm (18.7°) the ratio ranged around 0.5. Similar ratio changes versus eccentricity were found if the ratio was calculated separately for the superior and inferior hemimeridian.

3.3. Center-to-center separations of RGC, C and estimated 'receptive fields'

The transformation of RGC densities by using displacement data to 'effective' RGC densities made it possible to compare the characteristics of the sampling mosaics of C and RGC. The separation of RGC based on 'effective' densities compensated for non-linear projection steeply increased with eccentricity before starting to level off at greater eccentricities from the fovea (Table 2, Fig. 6). In contrast, the cone separation increased at a lower rate outside the foveal border.

Since more than one RGC receives information from the same foveal cone, RGC separation in the central retina will be smaller than the separation of cones. Each of the morphologically and functionally separate populations of RGC (such as midget-ON, midget-OFF and other types) constitute a separate mosaic of dendritic fields, each with total coverage of the retinal surface (Dacey, 1993). It is therefore more appropriate to examine the area from which one RGC receives information independently of the type of RGC. We have called this area the estimated 'receptive field'. In order to calculate density and separation of such 'receptive fields' we have divided 'effective' RGC density by the central RGC:C ratio (2.93) at all eccentricities. A curve describing such an estimate of center-to-center separation of 'receptive fields' versus eccentricity is given in Fig. 6b. As can be seen, the two curves diverge with increasingly lower C separation values at increasing eccentricities compared to corresponding estimated 'receptive field' separation values. It should be noted that this estimate of 'receptive field' separation does not take into account features such as changes in the proportion between different RGC types.

3.4. Separation and spatial resolution

The correction for lateral displacement of RGC from their corresponding cones and subsequent areal compensation gives 'effective' RGC separation values. The relationship between these 'effective' RGC separations and resolution thresholds, expressed in the same unit, can then be examined. According to the theory of proportionality this relationship should be linear through origin (for discussion see Frisén, 1995).

Perimetry results from additional measurements and those reported by Frisén (1992) describe the MAR values from 0 to 50° eccentricity along the vertical meridian of the same observers (Table 3). Thresholds were calculated for eccentricities corresponding to those in Tables 1 and 2 by linear interpolation and are shown in Table 3. A comparison of 'effective' RGC separation

Table 2
Cone, 'effective' RGC separation and (S.E.M.) data at corresponding eccentricities[a]

Eccentricity		Separation (min arc)					
mm	Degree	Cones			'Effective' RGC[b]		
		Case 1	Case 2	Case 3	Case 1	Case 2	Case 3
0.6	2.2	1.46[c]	1.57 (0.07)	1.31 (0.11)	0.90[c]	0.96[c]	1.08[c]
0.8	3.0	1.81 (0.10)	1.68 (0.09)	1.58 (0.08)	1.03[c]	1.02[c]	1.10[c]
1.6	6.0	1.90 (0.12)	1.98 (0.13)	1.93 (0.11)	1.45[c]	1.43[c]	1.48[c]
2.4	9.0	2.32 (0.18)	2.27 (0.18)	2.24 (0.19)	2.14 (0.15)	2.53 (0.17)	2.10 (0.13)
3.0	11.2	2.50 (0.21)	2.35 (0.15)	2.24 (0.17)	2.78 (0.32)	2.57 (0.23)	2.01 (0.15)
5.0	18.7	2.63 (0.22)	2.77 (0.27)	2.66 (0.30)	3.82 (0.48)	3.41 (0.32)	3.77 (0.61)
7.0	26.2	2.77 (0.28)	2.98 (0.24)	2.83 (0.27)	3.39 (0.42)	4.07 (0.82)	3.37 (0.30)
9.0	33.7	3.10 (0.28)	3.26 (0.29)	2.83 (0.23)	4.58 (0.75)	4.57 (0.68)	4.06 (0.51)

[a] Separation values are calculated from density values assuming hexagonal packing and transformed to cells/deg^2 according to Drasdo and Fowler (1974).

[b] Separation calculated from 'effective' RGC density, i.e. RGC density adjusted for displacement and areal change (cf Section 2).

[c] Based on interpolated density data.

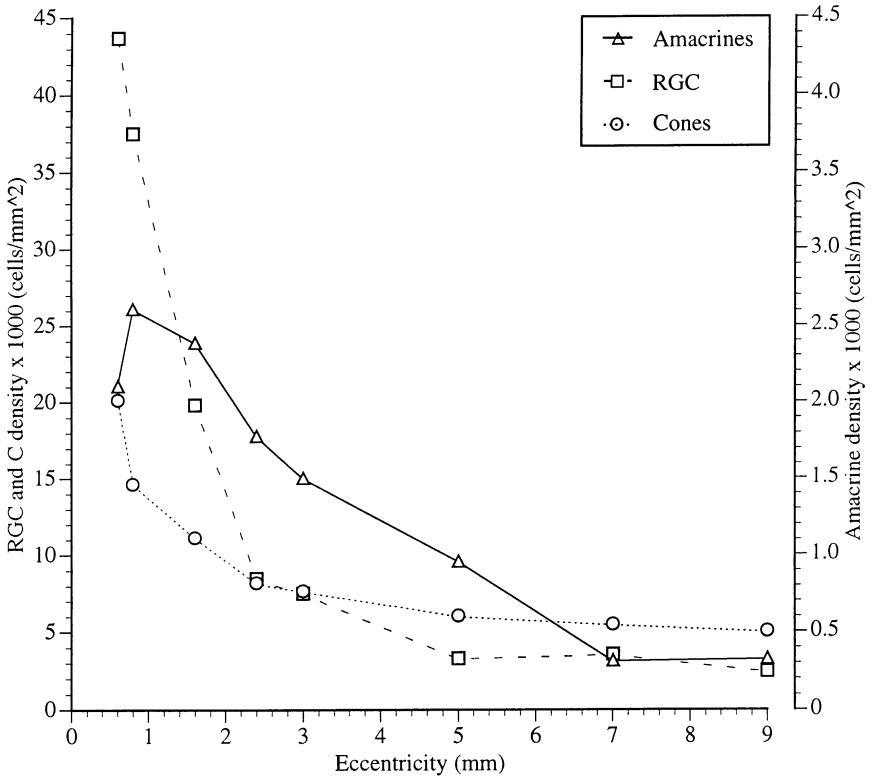

Fig. 4. Mean densities of RGC and cones (left y-axis) and displaced amacrine cells (right y-axis) of Case 1, 2 and 3 along the vertical meridian (mean of superior and inferior hemimeridians; cf. Table 1).

(Table 2) to interpolated resolution thresholds (Table 3) at corresponding eccentricities along the vertical hemimeridians is presented in Fig. 7a. The relationship was well fitted by quadratic functions when resolution thresholds were measured at both 0.5 (Fig. 7a) and 0.25 contrast (results not shown). The 'effective' RGC separation and MAR values for the central retina out to 5.0 mm (18.7°) eccentricity may be well fitted with a linear function (correlation coefficient of 0.98) with more peripheral values showing non-linearity. Fig. 7b presents the separation of C, 'effective' RGC and estimated 'receptive field' centers together with the calculated MAR thresholds (dash-dotted line) at a contrast of 90% (Frisén, 1995), as functions of eccentricity (Table 3). At 0.6 mm (2.2°) eccentricity, separation of C and estimated 'receptive field' centers are the same, as expected. These separation values at 0.6 mm are in close correspondence with those of MAR at 90% contrast whereas the RGC separation would predict a resolution better than transformed MAR. Outside the foveal border C and 'effective' RGC separations deviate from MAR, whereas the curve for separation of estimated 'receptive field' centers closely follows that of MAR out to 3.0 mm (11.2°) eccentricity.

On the basis of our quantitative estimates schematic models of circuitries from the cones to RGC were constructed for cone eccentricities extending from the fovea to the peripheral retina (Fig. 8). At the fovea a single cone connects to one ON and one OFF midget RGC (left diagram, Fig. 8a) whereas in the periphery several cones have connections to such an ON/OFF midget RGC pair (Fig. 8b). In correspondence, the receptive field subserved by an ON/OFF midget RGC pair is assumed to be represented by one cone in the fovea (left diagram, Fig. 8a) and a mosaic consisting of four to six cones in the periphery (Fig. 8b).

4. Discussion

The present study confirms an RGC:C ratio of about 3 in the human fovea (Sjöstrand et al., 1994) and demonstrates a rapid change in RGC:C circuitry outside the fovea. RGC outside the fovea relay information from more than one cone (i.e. cone convergence on RGC) in agreement with other quantitative morphological studies (Wässle et al., 1990). Separation of RGC steeply increases with eccentricity and a proportionality is found between RGC separation and resolution thresholds out to an eccentricity of at least 18.7° along the vertical meridian. We have demonstrated a close correspondence between center-to-center separation of estimated 'receptive fields' and spatial resolution within the central retina in humans.

Frisén (1992) has compared his resolution data, obtained by high-pass resolution perimetry, to ganglion

cell separation calculated from human ganglion cell densities reported by Curcio and Allen (1990). At an eccentricity of 10° or more, a proportionality was found for these parameters along the vertical meridian. Frisén's findings support a resolution model based on classical resolution theory, where a strict proportionality exists between resolution thresholds and their standard deviation and ganglion cell separation (Frisén, 1992, 1995). The present study with RGC data of the central retina, compensated for displacement and areal changes, support and extend these findings to the central retina.

There are previous neuroanatomical and physiological reports indicating that the mosaic of midget cells or cells projecting to the parvocellular layers of LGN is the cell substrate that limits spatial resolution (Dacey & Petersen, 1992; Croner & Kaplan, 1995). In the present study we made an attempt to correlate visual resolution thresholds with center-to-center separation of the whole RGC population expressed in the same unit, min of arc. Inherent difficulties in the analysis of the foveal center, i.e. large inter-individual differences, lack of blue cones within the foveola (Curcio & Allen, 1990; Curcio et al., 1990; Curcio, Allen, Sloan, Lerea, Hurley, Klock & Milam, 1991) and inaccuracies in definition of the foveolar center, were avoided in the present study by excluding the fovea inside 0.6 mm (2.2°) eccentricity from cell counting.

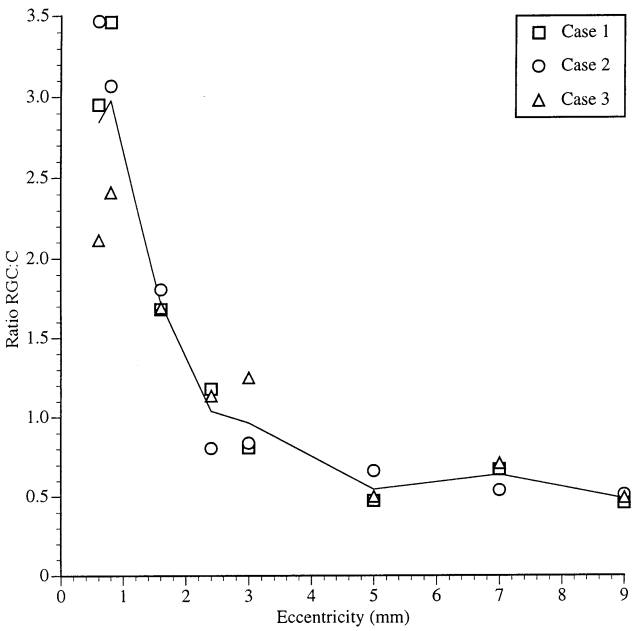

Fig. 5. RGC:C ratio versus eccentricity calculated as the ratio between 'effective' RGC density and cone density at corresponding locations for each case (cf. Fig. 3b). Mean values of the three cases are connected by the continuous line. The mean ratio is approx. 3 at the foveal border and falls below 1 at an eccentricity of 3 mm (11.2°).

A linearity could be shown between separation of RGC and resolution thresholds in the central retina. The center-to-center separation of the total RGC population predicts a Nyquist limit of resolution better than measured when compensated for suboptimal contrast of the high-pass filtered target (Frisén, 1995). Using the theoretically more appropriate measure of separation of detectors, the estimated 'receptive field', a closer correlation between resolution and separation is predicted. In agreement, Hirsch and Curcio (1989) found that the Nyquist limits determined by using cone counts within the human fovea offered a reasonable prediction of human acuity. However, calculations based on the cone mosaic cannot be used outside the fovea due to cone convergence (for discussion see Dacey, 1993) as illustrated by our RGC:C ratio and deviations of separation curves (Fig. 7b). Outside an eccentricity of approx. 11–20°, a non-linear relationship was found between separation of estimated 'receptive fields', RGC and MAR. Several factors may account for this finding, as discussed above. A decreasing proportion of midget to total RGC in the peripheral retina may be a major factor (Dacey, 1993). However, the uncertainty and increased spread of values in our study outside 5.0 mm (18.7°) eccentricity (see below) may also be a factor. Future studies aiming to define the proportion of midget to parasol cells are needed to clarify this problem.

Other previous studies of retinal cell separation and spatial resolution in humans and non-human primates have indicated that resolution of the central retina is limited by the separation of cone photoreceptors (Coletta & Williams, 1987; Hirsch & Curcio, 1989), whereas beyond about 10° eccentricity, the cone sampling frequency exceeds that of psychophysical measurements (Thibos, Cheney & Walsh, 1987; Merigan & Katz, 1990; Frisén, 1995). In contrast, our cell data indicate that cone convergence, i.e. an RGC:C value below 2, starts from an eccentricity of approx. 5° with an increasing discrepancy between cone separation and resolution thresholds. Similarly, Wässle et al. (1990) presented RGC:C values below 2 for macaque retina outside 3° temporally.

Our findings are in agreement with a similar study of one macaque (Wässle et al., 1990) and one human retina (Case 1, Sjöstrand et al., 1994). There is a steep decline in RGC:C ratio to unity within a limited eccentricity range (6.0–9.0°) reflecting marked changes in cone to ganglion cell circuitry outside the fovea. Morphological studies of human midget ganglion cells also show marked changes in dendritic field morphology outside the central 7.5° area (Rodieck et al., 1985; Kolb et al., 1992; Dacey, 1993; Goodchild, Ghosh & Martin, 1996).

Our models based on quantitative estimates of the connections between cones and RGC show the rapid

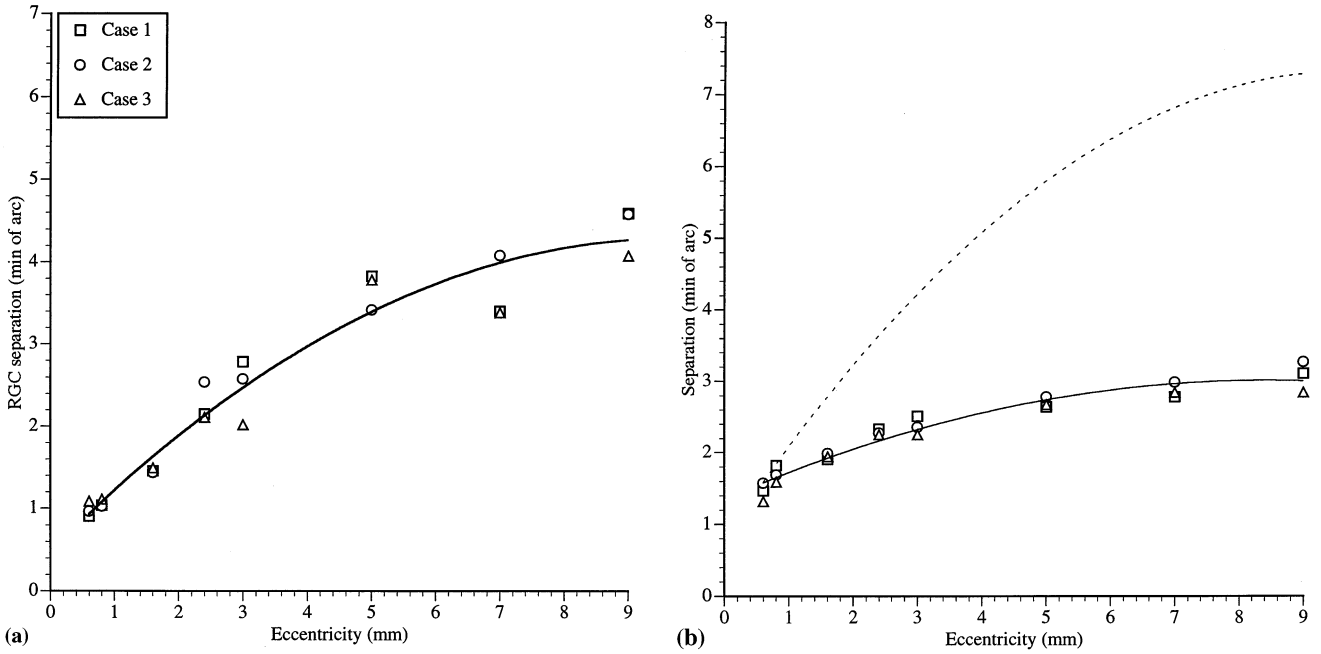

Fig. 6. The graphs show individual data as well as a best curve fit (continuous line) for (a) 'effective' RGC separation and (b) cone separation versus eccentricity (mean of data from superior and inferior hemimeridians with compensation for non-linear projection of the retinal image (Drasdo & Fowler, 1974)). In (b) the separation based on estimated 'receptive field' density versus eccentricity is indicated by the interrupted line (calculation, cf. text). Since it can be assumed that there are several separate dendritic mosaics made up of different types of RGC, the density of estimated 'receptive fields' was calculated by dividing the 'effective' RGC density by the central RGC:C ratio of 2.93. In the fovea, the size of one such estimated 'receptive field' will be equal or very close to the size of one cone, whereas in the periphery it will depend on the area including the cones connected to one RGC.

change of cone convergence, from one cone served by three RGC in the fovea to a corresponding number of six cones served by three RGC at an eccentricity of 18.7°. In comparison, Goodchild et al. (1996) similarly conclude that midget ganglion cells of the primate central retina derive their input from a single cone. In the periphery their macaque data demonstrate a cone to midget cell convergence increasing from approx. eight cones/cell between 20 and 30° to 22 cones/cell between 50 and 60°.

Some discrepancy exists between our RGC densities along the vertical meridian and those previously reported by Curcio and Allen (1990) using unstained whole mounts. The studies agree in the 6.0–11.2° eccentricity range, but our density values are higher at the foveal border and at more peripheral eccentricities. While the difference centrally may be explained by methodological difficulties related to cell counting in the foveal wall in whole mounts, one of the major problems in the periphery is distinguishing ganglion cells from displaced amacrines. In the present study we have approached the latter problem by using GABA-immunocytochemistry, reported to be a reliable marker for labeling displaced amacrine cells in primate retina (Wässle et al., 1990; Koontz et al., 1993). Still, this cannot explain the differences between our peripheral RGC results and those of Curcio and Allen, since we find higher amacrine cell densities (on average 19% between 11.2 and 33.7°) than Curcio and Allen (1990) (3% at 18.7°).

The use of vertical sections, and the disector method, enabled us to make estimates in very limited areas, without the loss of resolution that may affect quantitations in thick cell layers in whole mounts. One of the limitations with the present technique, however, is that of producing sufficient numbers of serial sections without altering the eccentricities. Due to this limitation, higher standard error of the mean (S.E.M.) values for individual eccentricities had to be accepted in the periphery. The coefficient of error for the separation values (CE, S.E.M./mean) was generally low out to 18.7°, but it was between 10 and 15% at eccentricities of 26.2 and 33.7°. However, a possible lack of precision in peripheral estimates did not affect the overall pattern of cell distribution, as judged by comparing the three retinae.

In conclusion, we have shown a close correspondence between separation of estimated 'receptive field' centers and spatial resolution in humans. High-pass resolution perimetry (HRP) thus allows for estimations of functional receptive fields within the central retina. The quantitative cell estimates allow us to present

Table 3
Minimum angle of resolution (MAR) measured with high-pass resolution perimetry[a]

Eccentricity	Measured MAR (min arc) contrast 0.5				Eccentricity		Interpolated MAR (min of arc) contrast 0.5 (0.9)			
Degree	Observer 1		Observer 2		mm	Degree	Observer 1		Observer 2	
	superior	inferior	superior	inferior			superior	inferior	superior	inferior
0.0[b]	1.3	1.3	1.1	1.1	0.6	2.2	1.9 (1.6)	2.0 (1.7)	1.3 (1.1)	1.6 (1.4)
2.5[b]	2.3	2.4	2.1	2.1	0.8	3.0	2.2 (1.8)	2.2 (1.9)	1.7 (1.4)	1.9 (1.6)
6.0[b]	3.0	3.1	3.1	3.4	1.6	6.0	3.3 (2.8)	3.2 (2.7)	3.0 (2.6)	3.0 (2.6)
10.0[b]	4.6	4.5	4.5	4.0	2.4	9.0	4.4 (3.8)	4.2 (3.6)	4.3 (3.7)	4.2 (3.6)
20.0[c]	9.1	8.1	8.5	6.4	3.0	11.2	5.3 (4.5)	4.9 (4 2)	5.3 (4.5)	5.0 (4.3)
30.0[c]	11.7	9.7	13.0	9.1	5.0	18.7	8.1 (7.0)	7.3 (6.3)	8.7 (7.4)	7.8 (6.6)
40.0[c]	15.4	14.5	15.5	15.3	7.0	26.2	11.0 (9.4)	9.8 (8.4)	12.0 (10.3)	10.6 (9.0)
50.0[c]	21.0	18.0	25.6	17.6	9.0	33.7	13.8 (11.8)	12.2 (10.4)	15.4 (13.2)	13.4 (11.4)

[a] Superior and inferior vertical meridian of two observers.
[b] Additional measurements.
[c] Calculations taken from Frisén, 1992.

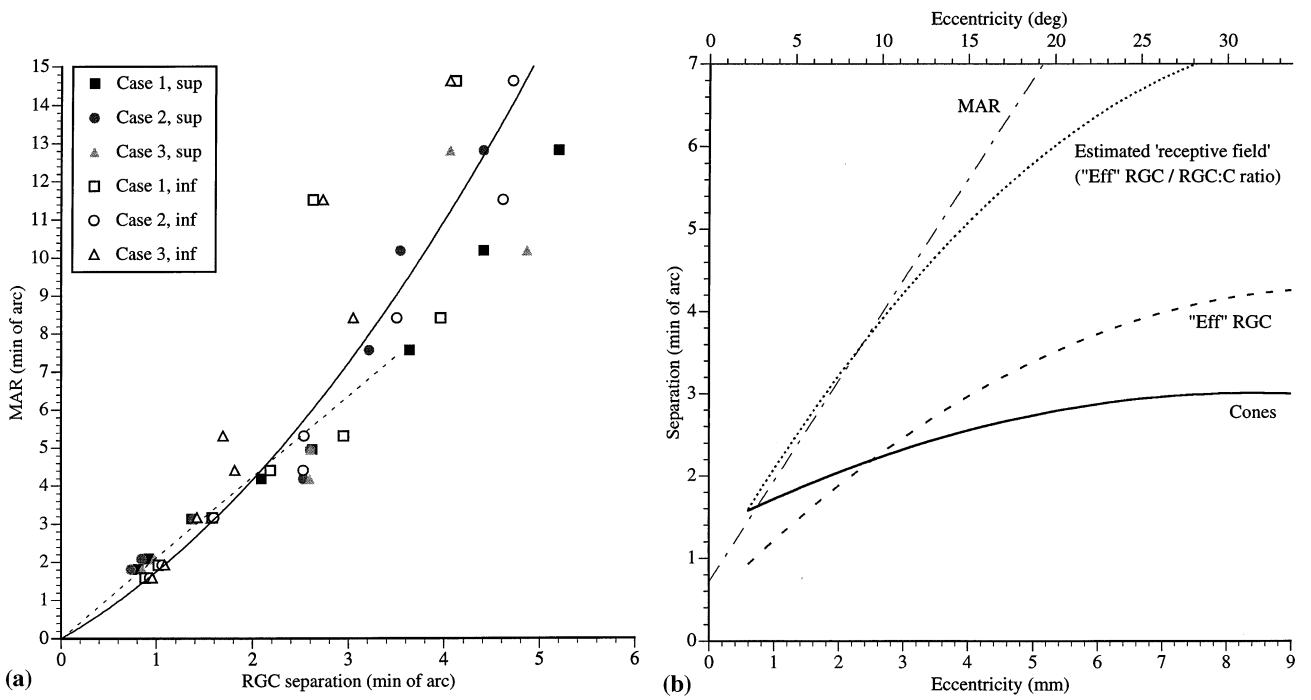

Fig. 7. (a) Minimum angle of resolution (MAR) threshold versus 'effective' RGC separation. 'Effective' RGC separations of Cases 1, 2 and 3 (Table 2) from the superior and inferior hemimeridians of the retina are plotted for each case against MAR thresholds (measured with 0.5 contrast (Table 3), mean of two observers) from the corresponding visual field. One outlying observation at 5.0 mm (18.7°) eccentricity was excluded. A quadratic function was fit to the data, $y = 0.30x^2 + 1.05x$ ($r = 0.94$). Linear regression equations out to 5.0 mm (18.7°, interrupted line) based on mean values and with origin constraint was $y = 1.76x$ ($r = 0.97$) for the function describing MAR versus 'effective' RGC separation. (b) Changes in separation of C (continuous line; from Fig. 6b), 'effective' RGC (dashed line; from Fig. 6a), and estimated 'receptive field' centers (dotted line; from Fig. 6b) together with MAR transformed to 90% contrast (dash-dotted line; from Table 3), with increasing eccentricity (shown as mm/°). As can be seen, the estimated 'receptive field' separation closely follows MAR to an eccentricity of 3 mm whereas separation of C and effective RGC diverge markedly. The larger deviation of C separation from MAR is presumably dependent on the fact that increasing numbers of cones are connected to the same RGC at higher eccentricities as indicated by the RGC:C ratio.

schematic models of the underlying C and RGC circuitries. For a further understanding of the structure and function of the human retina a quantitative separation of different RGC types is of importance.

Acknowledgements

This study was supported by the Swedish Medical Research Council (grants No. 02226, 07121) and a

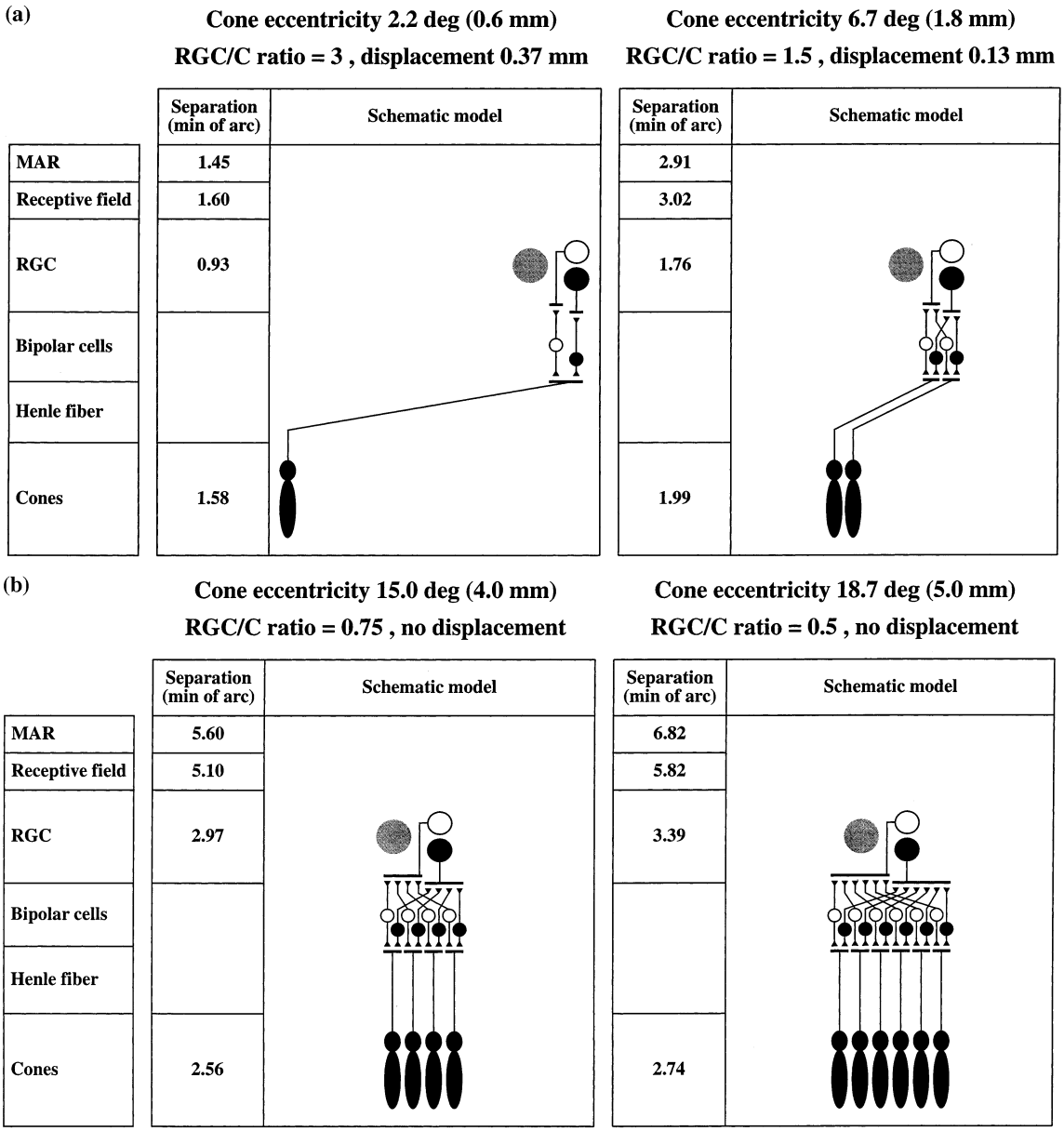

Fig. 8. Models of (a) central and (b) peripheral retinal circuitry (ON mosaics—open symbols, OFF mosaics—filled symbols) together with data on RGC:C-ratio, displacement, MAR (90% contrast), estimated 'receptive field' separation, 'effective' RGC separation and cone separation. We assume that in humans, out to 9 mm eccentricity, each cone is served by one ON and one OFF midget bipolar cell (Martin & Grünert, 1992) and independent sampling mosaics (Schiller, 1992), i.e. receptive fields. Based on the central RGC:C ratio of approx. 3, we have used relative proportions of midget to other RGC types (gray) of 2:1 at all eccentricities in order to simplify the diagrams; more accurate values can be obtained from Sterling, Calkins, Klug, Schein and Tsukamoto (1994) and Dacey (1993), respectively. No connections are indicated for RGC types other than midget ON and OFF. In the foveal region, the separation between cones is very similar to that of the estimated 'receptive field' centers and both may be regarded to limit spatial resolution. At eccentricities of 6.7, 15 and 18.7°, the separation of estimated 'receptive field' centers is larger than that of individual cones. The RGC:C ratio implies that each estimated 'receptive field' corresponds to two, four and six cones, respectively. Cones have schematically been drawn in one line but are in fact contained within the area of the receptive field.

grant from the Royal Society of Arts and Sciences in Göteborg. Thanks to Lars Frisén for providing the psychophysical data and for helpful discussions.

References

Bancroft, J. D., & Cook, H. C. (1994). *Manual of histological techniques and their diagnostic application* (pp. 63–64). London: Churchill & Livingstone.

Coletta, N. J., & Williams, D. R. (1987). Psychophysical estimate of extrafoveal cone spacing. *Journal of the Optical Society of America A*, *4*, 1503–1513.

Conradi, N., & Sjöstrand, J. (1993). A morphometric and stereologic analysis of ganglion cells of the central human retina. *Graefe's Archive for Clinical and Experimental Ophthalmology*, *231*, 169–174.

Croner, L. J., & Kaplan, E. (1995). Receptive fields of P and M ganglion cells across the primate retina. *Vision Research*, *35*, 7–24.

Curcio, C. A., Sloan, K. R., Kalina, R. E., & Hendrickson, A. E. (1990). Human photoreceptor topography. *Journal of Comparative Neurology*, *292*, 497–523.

Curcio, C. A., & Allen, K. A. (1990). Topography of ganglion cells in human retina. *Journal of Comparative Neurology*, *300*, 5–25.

Curcio, C. A., Allen, K. A., Sloan, K. R., Lerea, C. L., Hurley, J. B., Klock, I. B., & Milam, A. H. (1991). Distribution and morphology of human cone photoreceptors stained with anti-blue opsin. *Journal of Comparative Neurology*, *312*, 610–624.

Dacey, D. M., & Petersen, M. R. (1992). Dendritic field size and morphology of midget and parasol ganglion cells of the human retina. *Proceedings of the National Academy of Sciences USA*, *89*, 9666–9670.

Dacey, D. M. (1993). The mosaic of midget ganglion cells in the human retina. *Journal of Neuroscience*, *13*, 5334–5355.

Drasdo, N., & Fowler, C. W. (1974). Non-linear projection of the retinal image in a wide-angle schematic eye. *British Journal of Ophthalmology*, *58*, 709–714.

Eins, S., & Wilhelms, E. (1976). Assessment of preparative volume changes in central nervous tissue using automatic image analysis. *Microscope*, *24*, 29–38.

Frisén, L. (1992). High-pass resolution perimetry. evidence for parvocellular neural channel dependence. *Neuro-ophthalmology*, *12*, 257–264.

Frisén, L. (1995). High-pass resolution perimetry: central-field neuroretinal correlates. *Vision Research*, *35*, 293–301.

Goodchild, A. K., Ghosh, K. K., & Martin, P. R. (1996). Comparison of photoreceptor spatial density and ganglion cell morphology in the retina of human, macaque monkey, cat, and the marmoset *Callithrix jacchus*. *Journal of Comparative Neurology*, *366*, 55–75.

Grünert, U., Greferath, U., Boycott, B. B., & Wässle, H. (1993). Parasol (Pa) ganglion-cells of the primate fovea: immunocytochemical staining with antibodies against GABAA-receptors. *Vision Research*, *33*, 1–14.

Hirsch, J., & Curcio, C. A. (1989). The spatial resolution capacity of human foveal retina. *Vision Research*, *29*, 1095–1101.

Kolb, H., & Dekorver, L. (1991). Midget ganglion cells of the parafovea of the human retina: a study by electron microscopy and serial section reconstructions. *Journal of Comparative Neurology*, *303*, 617–636.

Kolb, H., Linberg, K. A., & Fisher, S. A. (1992). The neurons of the human retina: a golgi study. *Journal of Comparative Neurology*, *318*, 147–187.

Koontz, M. A., Hendrickson, L. E., Brace, S. T., & Hendrickson, A. E. (1993). Immunocytochemical localization of GABA and glycine in amacrine and displaced amacrine cells of macaque monkey retina. *Vision Research*, *33*, 2617–2628.

Martin, P. R., & Grünert, U. (1992). Spatial density and immunoreactivity of bipolar cells in the macaque monkey retina. *Journal of Comparative Neurology*, *323*, 269–287.

Merigan, W. H., & Katz, L. M. (1990). Spatial resolution across the macaque retina. *Vision Research*, *30*, 985–991.

Perry, V. H., & Cowey, A. (1984). Retinal ganglion cells that project to the superior colliculus and pretectum in the macaque monkey. *Neuroscience*, *12*, 1125–1137.

Rodieck, R. W., Binmoeller, K. F., & Dineen, J. (1985). Parasol and midget ganglion cells of the human retina. *Journal of Comparative Neurology*, *233*, 115–132.

Rodieck, R. W. (1998). *The first steps in seeing*. Sunderland, MA: Sinauer Associates, Inc.

Schein, S. J. (1988). Anatomy of macaque fovea and spatial densities of neurons in foveal representation. *Journal of Comparative Neurology*, *269*, 479–505.

Schiller, P. (1992). The on and off channels of the visual system. *Trends in Neuroscience*, *15*, 86–92.

Sjöstrand, J., Conradi, N., & Klarén, L. (1994). How many ganglion cells are there to a foveal cone? *Graefe's Archive for Clinical and Experimental Ophthalmology*, *232*, 432–437.

Snyder, A. W., & Miller, W. H. (1977). Photoreceptor diameter and spacing for highest resolving power. *Journal of the Optical Society of America*, *67*, 696–698.

Sterio, D. C. (1984). The unbiased estimation of number and sizes of arbitrary particles using the disector. *Journal of Microscopy*, *134*, 127–136.

Sterling, P., Calkins, D. J., Klug, K. J., Schein, S. J., & Tsukamoto, Y. (1994). Parallel pathways from primate fovea. *Investigative Ophthalmology & Visual Science* , 4, *35*, 3447.

Thibos, L. N., Cheney, F. E., & Walsh, D. J. (1987). Retinal limits to the detection and resolution of gratings. *Journal of the Optical Society of America A*, *4*, 1524–1529.

Wässle, H., Grünert, U., Röhrenbeck, J., & Boycott, B. B. (1990). Retinal ganglion cell density and cortical magnification factor in the primate. *Vision Research*, *30*, 1897–1911.

Wässle, H., Grünert, U., Martin, P. R., & Boycott, B. B. (1994). Immunocytochemical characterization and spatial distribution of midget bipolar cells in the macaque monkey retina. *Vision Research*, *34*, 561–579.